arXiv:1403.6244v1 [astro-ph.HE] 25 Mar 2014

Analysis of short bursts in SGR 1806-20, 1E 1048-5937 and SGR 0501+4516

Zhijie Qu[1], Zhaosheng Li[1], Yupeng Chen[2], Shi Dai[1], Long Ji[2], Renxin Xu[1,3], Shu Zhang[2]

ABSTRACT

We analyzed the temporal and spectral properties, especially the short bursts, for three anomalous X-ray pulsars (AXPs) and soft gamma repeaters (SGRs), including SGR 1806-20, 1E 1048-5937 and SGR 0501+4516. Using the data from *XMM-Newton*, we located the short bursts through Bayesian blocks algorithm. The short bursts duration distributions for three sources were fitted by two log-normal functions, however, the spectra of shorter bursts (< 0.2 s) and longer bursts (≥ 0.2 s) can be well fitted by two black body components with different emission areas for SGR 0501+4516. We studied the flux evolution of the persistent and the burst emission, and found a similar tendency of flux during outburst. We also found that there is a positive correlation between the burst luminosity and the persistent luminosity with a power law index $\gamma = 1.22 \pm 0.19$. The ratio of this persistent emission to the time averaged short bursts is in the range of $10 \sim 10^3$, similar to the case in Type I X-ray burst. In the end, we discussed our results in the accretion model and magnetar model for AXPs and SGRs.

Subject headings: pulsars: individual (SGR 1806-20, 1E 1048-5937, SGR 0501+4516) - stars: neutron - X-rays: bursts

1. Introduction

Anomalous X-ray pulsars (AXPs) and soft gamma repeaters (SGRs) are isolated neutron stars. They have long rotation periods ($2 \sim 10$ s) and rapid spin-down rates ($10^{-13} \sim$

[1]School of Physics and State Key Laboratory of Nuclear Physics and Technology, Peking University, Beijing 100871, P. R. China

[2]Institute of High Energy Physics & Theoretical Physics Center for Science Facilities, Chinese Academy of Sciences, Beijing 100049, China

[3]Kavli Institute for Astronomy and Astrophysics, Peking University, Beijing 100871, P. R. China

10^{-11} s s^{-1}) compared with radio pulsars. Their soft X-ray luminosity is about $10^{34} - 10^{36}$ erg s^{-1}, which far exceeds their rotational energy loss rates (Mereghetti 2008). Assuming magnetic dipole braking a vacuum, their characteristic magnetic field can exceed the quantum critical value ($B_{\rm QED} = 4.4 \times 10^{13}$ G). Observationally, AXPs/SGRs have many kinds of activities, such as, outbursts and bursts, pulse profile changes as well as timing anomalies (glitch and anti-glitch).

Duncan & Thompson (1992) firstly raised the "magnetar" concept and discussed the formation of a magnetar. They suggested that an $\alpha\Omega$ dynamo operating in neutron star with initial period $P \sim 1$ ms could generate a dipole magnetic field much stronger than 10^{13} G. Thompson & Duncan (1996) considered the persistent radiation of AXPs/SGRs as a result of a magnetic field decay and the persistent seismic activity, producing low amplitude Alfvén waves in the magnetosphere, as an effective origin of the X-ray emission. Several proposals under the magnetar framework have been established to explain bursts, e.g., strong magnetic reconnection (Lyubarsky et al. 2002) and magnetic pressure triggered crust fractures (Heyl & Hernquist 2005). However, some challenges are inevitably raised up, such as, the existence of low magnetic field magnetars (SGR 0418+5729, Rea et al. 2013; Swift J1822.31606, Rea et al. 2012; 3XMM J185246.6+003317, Rea et al. 2014, Zhou et al. 2014), and the prediction, that magnetar should have large spatial velocities and energetic associated supernovae, made by Duncan & Thompson (1992) have not been observed yet (Mereghetti 2008).

The accretion disk model, which is widely accepted in binary systems, was raised up for AXPs/SGRs in a form of fossil disk, in which the emission is powered by accretion from the disk (Chatterjee et al. 2000). Wang et al. (2006) observed the fallback disk of 4U 0142+61 directly, where the disk may come from a supernova fallback origin. However, this disk shows no accretion process. The accretion-based models were usually criticized because the lack of mechanism to explain the giant flares and bursts, which indicate that these models must look for help from magnetar model to become a "hybrid" and complete model (Mereghetti 2008). Nevertheless, combining the accretion model and strange matter state, Xu and coworkers (Xu 2003; Zhou et al. 2004; Xu et al. 2006; Xu 2007) suggested that the solid quark stars, instead of neutron stars, could generate giant flares and bursts in the process of accretion-induced star-quakes. Also a solid state of quark matter could be helpful to understand the plateau of gamma-ray burst (Dai et al. 2011).

Cheng et al. (1996) discovered the similarity between the short bursts in SGR 1806-20 and the earthquakes, based on the power law energy distributions $dN \propto E^{-1.6\pm0.2}dE$ and log-symmetric waiting time distributions. Then more systemic statistics were done for SGR 1900+14 (Göğüş et al. 1999) and SGR 1806-20 (Göğüş et al. 2000). Göğüş and coworkers

showed the burst fluence distributions with a power law index ~ 1.66 for SGR 1900+14 and ~ 1.6 for SGR 1806-20. They found lognormal distribution of waiting time for each source, peaked at ~ 49 s for SGR 1900+14 and ~ 97 s for SGR 1806-20. Moreover, they concluded that there is no relationship between the burst strength and the waiting time. Göğüş et al. (2001) discovered the lognormal distribution of the short burst duration with the value peaked at ~ 0.1 s. In recent years, Prieskorn & Kaaret (2012) discussed the fluence distribution for SGR 1806-20 and SGR 1900+14 using all the *RXTE* observations and claimed that the distributions should be a broken power law with exponential cutoff. Lin et al. (2012) researched the dimmer short bursts spectrum and concluded that the persistent radiation could not have the same origin with dim short bursts. Although many researchers have found short bursts from AXPs (Gavriil et al. 2002; Kaspi et al. 2003; Gavriil et al. 2008), no statistic works have been done for AXPs. Benefiting from Bayesian blocks algorithm, we could search more short bursts in AXPs and compare the properties of bursts in SGRs.

Bayesian blocks algorithm was developed by Scargle (1998) and Scargle et al. (2013) to analyze the structures in photon counting data and to detect Gamma-ray Bursts. Lin et al. (2013) firstly used this algorithm to search short bursts in SGRs. It shows a great efficiency in distinguishing the dim bursts. They analyzed the morphological properties of the short bursts and fitted the duration distributions with two lognormal functions for SGR 0501+4516, and then verified the power law distribution of fluence.

In Section 2, we describe the observations and data reduction. The details of detecting short bursts by using Bayesian blocks algorithm are presented in Section 3. In Section 4, we show that the short burst duration distributions, evolution of the flux and the relationship between short bursts and persistent emission. In the end, the discussion about accretion model and the magnetar model, based on our results, is available in Section 5.

2. Observations and data reduction

We chose three sources for our researches, including SGR 1806-20, 1E 1048-5937 and SGR 0501+4516. The data were observed by *XMM-Newton* space telescope. All these sources have enough observations to research short bursts statistically.

SGR 1806-20 is one of the earliest SGRs which was discovered in 1978 and confirmed in 1987 (Laros et al. 1987). It is also one of the most energetic sources among all AXPs/SGRs. In December 2004, it showed the third giant flare (Borkowski et al. 2004) in all SGRs. It released $\sim 10^{46}$ erg during ~ 0.5 s (Mereghetti 2008). *XMM-Newton* implemented about 10 years monitoring and observed its entire outburst variation. 1E 1048-5937 is a bright AXP,

had experienced two outbursts in 2002-2004 and 2007 (Tam et al. 2008). *XMM-Newton* have one observation for each outburst respectively. SGR 0501+4516 was discovered on 2008-8-22, when it entered in its first outburst (Barthelmy et al. 2008). *XMM-Newton*'s observation began on 2008-8-23, showing an entire outburst decay similar to that of SGR 1806-20.

We analyzed the data from detector PN on board *XMM-Newton*, since it has the highest time resolution among all three soft X-ray detectors. Almost all of the observations are in the imaging modes, only one observation for 1E 1048-5937 is in timing mode. We only used the data in imaging mode, to make the results from different observations comparable. We circled the region with radius $30''$ centered on sources position and $45''$ for backgrounds aside these sources, then obtained the time-tagged events (TTE) data. Using these TTE data, we located the short bursts by Bayesian blocks algorithm. The details about the Bayesian blocks algorithm will be discussed in Section 3.

In order to compute the flux and luminosity, we fitted the persistent spectrum for each observation and burst spectra for the observations with more than 50 burst photons. We adopted absorbed black body plus power law (**phabs(bbodyrad+powerlaw)** in Xspec) for the persistent emissions and a single absorbed black body for bursts, an extra black body component is added if necessary. The photoelectric absorption parameter $N_{\rm H}$ were fixed using the value from magnetar catalog (Olausen & Kaspi 2013) shown in Table 1, except the observations of SGR 0501+4516 shown in Table 5. Examples for the persistent and the burst spectrum are shown in Fig. 1 respectively. After the spectral fitting, the *cflux* in Xspec was used to calculate the unabsorbed flux in the energy band $1.0 - 10.0$ keV and the error with 90% confidence range. To obtain the luminosity in the same band, we used the distance in Table 1. The results are listed in Table 2 - Table 5.

3. Details of locating short bursts

In Bayesian blocks algorithm, the optimal block partition is obtained by maximizing the likelihood function (L) (Scargle et al. 2013),

$$\ln L^{(k)} = N^{(k)} \ln \lambda^{(k)} - \lambda^{(k)} T^{(k)}, \tag{1}$$

where $N^{(k)}$, $\lambda^{(k)}$, $T^{(k)}$ are the total number of photons, expected count rate and duration of the block k, respectively. The algorithm depends on the prior blocks distribution index (*ncp_prior*) and false positive probability p_0. We utilized the equation (21) in Scargle et al. (2013) ($ncp_prior = 4 - \log(73.53 p_0 N^{-0.478})$) to determine *ncp_prior* and chose 0.05 as the default value of p_0.

Although the time complexity have been reduced to $O(n^2)$ (Scargle et al. 2013), it is

still an unacceptable computing time if we apply the Bayesian blocks algorithm to the entire observation. To reduce the time complexity again, we divided the entire observation into several segments with equal length. For different sources, we defined the length as the bigger one between 50 times the mean rate and 100 cts s^{-1}.

To decrease the effect of the different separations, we set two rounds detection as suggested by Lin et al. (2013). The first round started from the beginning of the observation and the second round was a half separation postponed compared to the first one. For each round, we applied the Bayesian blocks algorithm to each segment, and obtained the raw change points. If one change point was also a discontinuity points we set in the separations, we used the two segments before and after it to determine whether it was a change point or not. We merged the two round results together and calculated the final rate for each block. We defined the blocks longer than double periods of the source are the background blocks. We amalgamated background blocks to estimate the background count rate level. After that, we tagged the blocks with rates higher than backgrounds as short burst blocks. Our results are shown in Table 2 and an example of the result of Bayesian blocks algorithm is shown in Fig. 2. All background blocks, for each observation respectively, are collected to constitute the persistent data, while the burst blocks are also collected as the burst data.

4. Results

4.1. The duration distributions

After locating the short bursts, we made the duration distributions for SGR 1806-20, 1E 1048-5937 and SGR 0501+4516. We found that each distribution can be well fitted using two lognormal functions. All the results are shown in Fig. 3. For SGR 1806-20, the two components are $\tau_1 = 122 \pm 6$ ms with standard deviation $\sigma_1 = 0.46 \pm 0.02$ and $\tau_2 = 4551^{+2062}_{-1419}$ ms with $\sigma_2 = 0.46 \pm 0.19$. For 1E 1048-5937, the two components are $\tau_1 = 819^{+115}_{-101}$ ms with $\sigma_1 = 0.68 \pm 0.06$ and $\tau_2 = 1651^{+64}_{-62}$ ms with $\sigma_2 = 0.20 \pm 0.03$. For SGR 0501+4516, the two components are $\tau_1 = 86^{+12}_{-10}$ ms with $\sigma_1 = 0.36 \pm 0.04$ and $\tau_2 = 817^{+330}_{-235}$ ms with $\sigma_2 = 0.52 \pm 0.10$. The $\chi^2/d.o.f$ are 1.00/4, 0.73/4 and 2.68/4, respectively.

Especially for the first observation of SGR 0501+4516 (Obs. ID 0560191501), Lin et al. (2013) accomplished the temporal analysis of the dim short bursts. To make a comparison with their results, we made the duration distribution for this observation specially, shown in Fig. 4. Our results showed that $\chi^2/d.o.f. = 9.97/7$ and two lognormal components of $\tau_1 = 83^{+19}_{-16}$ ms with $\sigma_1 = 0.37 \pm 0.06$, as well as $\tau_2 = 744^{+802}_{-386}$ ms with $\sigma_2 = 0.56 \pm 0.20$, while Lin et al. (2013) showed that $\chi^2/d.o.f. = 3.65/5$ and two lognormal components of

$\tau_1 = 85 \pm 8$ ms with $\sigma_1 = 0.36 \pm 0.03$, and $\tau_2 = 1028^{+220}_{-181}$ ms with $\sigma_2 = 0.32 \pm 0.05$. Since the Bayesian block algorithm have some prior parameters, we get the different bursts sample compared to Lin et al. (2013). However, considered the uncertainties, our results are consistent with Lin et al. (2013).

We noticed that for SGR 1806-20 and SGR 0501+4516, the bursts are mainly dominated by the shorter time scale bursts ($\sim$ 0.1 s), while for 1E 1048-5937, the longer time scale bursts ($\sim$ 1 s) are in the majority. To investigate the spectral properties of short time scale bursts and long time scale bursts, we divided the bursts into two subclass at 0.2 s for SGR 0501+4516, since SGR 0501+4516 has enough burst photons for spectral fitting and 0.2 s is the approximate intersecting point of the two components. Both spectra can be well fitted by two black body components or the optical thin thermal bremsstrahlung (OTTB) model, shown in Fig. 5. Fitting these two spectra for longer or shorter bursts in two black bodies model, respectively, the two components are 0.62 ± 0.04 keV and $2.53^{+0.40}_{-0.29}$ keV with reduced $\chi^2 = 1.02(221)$, or $0.57^{+0.09}_{-0.08}$ keV and $2.00^{+0.61}_{-0.33}$ keV with reduced $\chi^2 = 1.19(111)$. The low energy bands (< 1.3 keV) of spectra are a little higher than the model, but the two reduced χ^2 show that these results are still acceptable. In OTTB model, the plasma temperatures are $23.49^{+5.22}_{-3.78}$ keV with reduced $\chi^2 = 1.02(223)$ or $20.94^{+9.93}_{-5.47}$ keV with reduced $\chi^2 = 1.14(113)$. Considering the uncertainly of characteristic temperatures, the main difference is the normalizations, which are the emission areas for black bodies or the densities of plasma for OTTB. Our results indicate that the bursts with duration less than 0.2 s have larger normalization no matter which model is used.

4.2. The flux evolution

From the spectral fitting results, we plotted the persistent flux ($F_{\rm p}$) and the average burst flux ($F_{\rm aver,b}$) evolution for SGR 1806-20, 1E 1048-5937 and SGR 0501+4516 in Fig. 6. The average burst flux denotes that the total burst fluence is averaged into an entire observation, so it represents the strength of burst energy releasing during this observation.

4.2.1. SGR 1806-20

SGR 1806-20 is the most special source among all three sources because of its giant flare, as we mentioned in Section 2. We noticed that the persistent flux experienced a decay, while the average burst flux showed fluctuation due to the giant flare. After the giant flare, the burst flux became much lower than earlier epoch within three months. And during next

two years, it lasted its low burst rate condition until late in 2006. After a weak peak around MJD 54000, the burst flux curve entered into another decay stage.

4.2.2. SGR 0501+4516

The persistent flux of SGR 0501+4516 showed a decay, while the average burst flux showed a steeper drop to the bottom. We separated the first observation into four segments. The persistent flux did not change significantly, while the average burst flux had an apparent peak at the second segment.

4.2.3. 1E 1048-5937

The flux evolution of this source did not appear a decay stage as SGR 1806-20 and SGR 0501+4516, because *XMM-Newton* did not have enough observations. According to Tam et al. (2008), 1E 1048-5937 had experienced two outbursts in 2002-2004 and 2007, so the flux variance showed a comparison between the outburst and the quiescent period.

4.3. Short bursts versus persistent emission

Based on the spectral fitting results, we analyzed the short bursts and the persistent emission properties for the sources. We adopted the flux and luminosity to estimate the strength of the short bursts and persistent emission simultaneously. In Fig. 7, We fitted $F_{\rm b}$ and $F_{\rm p}$ using a power law,

$$F_{\rm b} \propto {F_{\rm p}}^{\gamma}, \tag{2}$$

with index $\gamma = 0.95 \pm 0.63$ and Pearson correlation coefficient $\rho = 0.41$. The fit result shows that there is a marginal positive correlation between the burst flux and the persistent flux. We also fitted the burst flux and the persistent flux using a power law with $\gamma = 1.22 \pm 0.19$ and $\rho = 0.89$ in Fig. 7. This correlation is more intrinsic than the flux one, which implies that there is a tight relationship between the short bursts and the persistent radiation.

Fig. 8 shows a scatter relation between the burst rate and the persistent flux for all the sources. The power law indices and correlation coefficients for SGR 1806-20, 1E 1048-5937 and SGR 0501+4516 are 2.18 ± 0.65, 0.51 ± 0.33, 1.63 ± 0.72 and $\rho = 0.78,\ 0.62,\ 0.75$, respectively. The relationship between the burst rate and $F_{\rm p}$ can be described as a power law with $\gamma = 1.23 \pm 0.36$ and $\rho = 0.62$. In Fig. 9, we computed the ratio $(L_{\rm p}/L_{\rm aver,b})$ and

found that the ratio is independent of the persistent luminosity, $\sim 10 - 1000$. Then we also fitted the ratio distribution with a lognormal fitting, shown in Fig. 9. The mean value of the ratio is $611^{+253.06}_{-178.96}$ and the standard deviation is 0.56 ± 0.12.

5. Conclusion and Discussion

In this paper, we showed the temporal and spectral results of short bursts using the Bayesian blocks algorithm for three AXPs/SGRs. We found the duration distributions for AXPs/SGRs can be fitted by two lognormal functions. Among all the three sources, the mean values of two components are $\sim$ 0.1 ms and $\sim$ 1 ms respectively. 1E 1048-5937 is dominated by longer time scale bursts, while SGR 1806-20 and SGR 0501+4516 by shorter ones. The spectrum analysis for longer and shorter time scale bursts showed no obviously difference, which implies that these two types burst may share a common origin.

We researched the relationship of luminosity between the short bursts and the persistent emission, which showed a power law with $\gamma = 1.22 \pm 0.19$. In accretion model, this phenomenon is natural, since the persistent radiation represents the accretion rate, while the burst radiation represents the accumulation of the accreted matter. In the magnetar model, both the persistent emission and the bursts are from the magnetic energy. During an outburst, some seismic activities may trigger magnetic reconnections or crystal fractures, which is responsible for the short burst (Thompson & Duncan 1996). During this process, the magnetosphere will become more twisted. The corresponding persistent flux will also increase (Beloborodov 2009).

We also claimed that the ratio ($L_{\rm p}/L_{\rm aver,b}$) is independent with $F_{\rm p}$ or $L_{\rm p}$, which could be comparable to that of Type I X-ray bursts (with ratios between $\sim$ 40 to few hundred, Galloway et al. 2008). Based on these results, we could speculate that the the short bursts from AXPs/SGRs and Type I X-ray bursts may arise from similar trigger mechanisms.

Nowadays, the popular mechanism for Type I X-ray burst is the unstable nuclear burning of the accreted matter. The base of the mechanism for outburst is the ineluctable conversion of a hydrogen-rich accreted matter to a neutron rich composition in the neutron star interior (Taam 1998). Addition to the outburst, the conversion is unstable, resulting in X-ray bursts, in a helium or a hydrogen-helium co-exist layer. However, Altamirano et al. (2012) found that the superburst from EXO 1745-248 is very challenging for current thermonuclear ignition models, because it is too cold to ignite a carbon burning in current models. Nevertheless, in the framework of the accretion scenario, where internal gravitational and elastic energy release during a quake of massive compact star might be responsible for triggering the bursts

(Xu et al. 2006), the constant ratio could be natural for both AXPs/SGRs and Type I X-ray bursters if a corona-like layer covers an accreting solid quark star (Xu 2014).

What's more, we noticed that two SGRs showing the entire decay of an outburst had similar performances: the persistent flux showed a normal decay apparently and the burst flux showed steep peaks. These steep peaks represent the ultra active phases, which for SGR 1806-20 is a giant flare while for SGR 0501+4516 is a period with frequent short bursts. However, there are also differences between these two sources. The burst flux of SGR 1806-20 had double ascent stages, while SGR 0501+4516 had only one. In the accretion model, it could be expected that accretion rate variation would be responsible for a long time-scale ($\sim 10^2$ days) luminosity change. In the first active phase of SGR 1806-20 (top-right plot in Fig. 6), the source may deplete all of the accumulated energy in the form of gravitational, elastic even nuclear energy. After that, SGR 1806-20 could enter in another accumulating-releasing cycle (i.e., the second active phase in the top-right plot of Fig. 6), since SGR 1806-20 had a slower decreasing accretion rate than SGR 0501+4516.

We would like to thank the pulsar group of PKU for helpful discussions and comments, and Hao Tong from XAO of CAS for supplements about magnetar model. This work is supported by the National Basic Research Program of China (Grant No. 2012CB821800), the National Natural Science Foundation of China (Grant Nos. 11225314, Grant Nos. 11133002, NSFC-11103020), National Found for Fostering Talents of Basic Science (No. J0630311), and XTP project XDA04060604, XDB09000000 (Supported by the Strategic Priority Research Program "The Emergence of Cosmological Structures" of the Chinese Academy of Sciences, Grant No. XDB09000000). This research is based on data and software provided by the the ESA *XMM-Newton* Science Archive (XSA) and the NASA/GSFC High Energy Astrophysics Science Archive Research Center (HEASARC).

REFERENCES

Altamirano, D., Keek, L., Cumming, A., et al. 2012, MNRAS, 426, 927

Barthelmy, S. D., Baumgartner, W. H., Beardmore, A. P., et al. 2008, The Astronomer's Telegram, 1676, 1

Beloborodov, A. M. 2009, ApJ, 703, 1044

Bibby, J. L., Crowther, P. A., Furness, J. P., & Clark, J. S. 2008, MNRAS, 386, L23

Borkowski, J., Gotz, D., Mereghetti, S., et al. 2004, GRB Coordinates Network, 2920, 1

Chatterjee, P., Hernquist, L., & Narayan, R. 2000, ApJ, 534, 373

Cheng, B., Epstein, R. I., Guyer, R. A., & Young, A. C. 1996, Nature, 382, 518

Dai, S., Li, L. X., & Xu, R. X. 2011, Science China-Physics Mechanics & Astronomy, 54, 1541

Dib, R., Kaspi, V. M., & Gavriil, F. P. 2009, ApJ, 702, 614

Duncan, R. C., & Thompson, C. 1992, ApJ, 392, L9

Durant, M., & van Kerkwijk, M. H. 2006, ApJ, 650, 1070

Galloway, D. K., Muno, M. P., Hartman, J. M., Psaltis, D., & Chakrabarty, D. 2008, ApJS, 179, 360

Gavriil, F. P., Dib, R., & Kaspi, V. M. 2008, in American Institute of Physics Conference Series, Vol. 983, 40 Years of Pulsars: Millisecond Pulsars, Magnetars and More, ed. C. Bassa, Z. Wang, A. Cumming, & V. M. Kaspi, 234–238

Gavriil, F. P., Kaspi, V. M., & Woods, P. M. 2002, Nature, 419, 142

Göğüş , E., Woods, P. M., Kouveliotou, C., et al. 1999, ApJ, 526, L93

Göğüş, E., Kouveliotou, C., Woods, P. M., et al. 2001, ApJ, 558, 228

Göğüş, E., Woods, P. M., Kouveliotou, C., et al. 2010, ApJ, 722, 899

—. 2000, ApJ, 532, L121

Heyl, J. S., & Hernquist, L. 2005, ApJ, 618, 463

Kaspi, V. M., Gavriil, F. P., Woods, P. M., et al. 2003, ApJ, 588, L93

Laros, J. G., Fenimore, E. E., Klebesadel, R. W., et al. 1987, ApJ, 320, L111

Leahy, D. A., & Tian, W. W. 2007, A&A, 461, 1013

Lin, L., Göğüş, E., Güver, T., & Kouveliotou, C. 2012, ApJ, 761, 132

Lin, L., Göğüş, E., Kaneko, Y., & Kouveliotou, C. 2013, ApJ, 778, 105

Lyubarsky, Y., Eichler, D., & Thompson, C. 2002, ApJ, 580, L69

Mereghetti, S. 2008, A&A Rev., 15, 225

Mori, K., Gotthelf, E. V., Zhang, S., et al. 2013, ApJ, 770, L23

Nakagawa, Y. E., Mihara, T., Yoshida, A., et al. 2009, PASJ, 61, 387

Olausen, S. A., & Kaspi, V. M. 2013, arXiv:1309.4167, 1309.4167

Prieskorn, Z., & Kaaret, P. 2012, ApJ, 755, 1

Rea, N., Vigan, D., Israel, G. L., Pons, J. A., & Torres, D. F. 2014, ApJ, 781, L17

Rea, N., Israel, G. L., Turolla, R., et al. 2009, MNRAS, 396, 2419

Rea, N., Israel, G. L., Esposito, P., et al. 2012, ApJ, 754, 27

Rea, N., Israel, G. L., Pons, J. A., et al. 2013, ApJ, 770, 65

Scargle, J. D. 1998, ApJ, 504, 405

Scargle, J. D., Norris, J. P., Jackson, B., & Chiang, J. 2013, ApJ, 764, 167

Taam, R. E. 1998, in American Institute of Physics Conference Series, Vol. 425, American Institute of Physics Conference Series, 551–558

Tam, C. R., Gavriil, F. P., Dib, R., et al. 2008, ApJ, 677, 503

Thompson, C., & Duncan, R. C. 1996, ApJ, 473, 322

Wang, Z., Chakrabarty, D., & Kaplan, D. L. 2006, Nature, 440, 772

Xu, R. 2003, ApJ, 596, L59

—. 2007, Advances in space research, 40, 1453

Xu, R. 2014, ArXiv e-prints, arXiv:1402.1290

Xu, R., Tao, D., & Yang, Y. 2006, MNRAS, 373, L85

Zhou, A., Xu, R., Wu, X., & Wang, N. 2004, Astroparticle Physics, 22, 73

Zhou, P., Chen, Y., Li, X.-D., et al. 2014, ApJ, 781, L16

This preprint was prepared with the AAS LaTeX macros v5.2.

Table 1: The parameters of sources.

Source	Period (s)	Epoch (MJD)	Ref.	Distance (kpc)	Ref.	$N_{\rm H}$ ($10^{22}{\rm cm}^{-2}$)	Ref.
SGR 1806-20	7.6022(7)	54189	(1)	$8.7^{+1.8}_{-1.5}$	(4)	6.9 ± 0.4	(7)
1E 1048-5937	6.4578754(25)	54185.9	(2)	9.0 ± 1.7	(5)	0.97 ± 0.01	(8)
SGR 0501-4516	5.76209653(3)	54750	(3)	0.8 ± 0.4	(6)	$0.6^{+0.5}_{-0.3}$	(9)

References. — (1)Nakagawa et al. (2009), (2)Dib et al. (2009), (3)Göğüş et al. (2010), (4)Bibby et al. (2008), (5)Durant & van Kerkwijk (2006), (6)Leahy & Tian (2007), (7)Mori et al. (2013), (8)Tam et al. (2008), (9)Rea et al. (2009)

Table 2: The short bursts results.

source	OBS-ID	$N_{\rm photon}$	$N_{\rm burst}$	source	OBS-ID	$N_{\rm photon}$	$N_{\rm burst}$
SGR 1806-20	0148210101	0	0	1E 1048-5937	0147860101	245	11
	0148210401	0	0		0307410201	77	7
	0164561101	771	28		0307410301	87	8
	0164561301	8	1		0510010601	544	25
	0164561401	47	6		0654870101	264	21
	0205350101	606	27	SGR 0501+4516	0552971101	204	7
	0406600301	24	1		0552971201	67	3
	0406600401	244	12		0552971301	139	7
	0502170301	59	6		0552971401	18	1
	0502170401	23	2		0560191501	10897	270
	0554600301	0	0		0560191501[1][a]	2854	72
	0554600401	0	0		0560191501[2][a]	3566	82
	0604090201	0	0		0560191501[3][a]	2732	67
	0654230401	5	1		0560191501[4][a]	2120	56
1E 1048-5937	0112780401	14	1		0604220101	20	2

[a]These four segments labeled as 1 to 4 are divided from the observation ID 0560191501.

Table 3: The spectral results of SGR 1806-20.

OBS-DATE	OBS-ID	persistent spectrum phabs(BB+PL)			burst spectrum phabs(BB)	
		kT(keV)	γ	$red.\chi^2(d.o.f.)$	kT(keV)	$red.\chi^2(d.o.f.)$
2003-04-03	0148210101	$0.44^{+0.13}_{-0.17}$	$1.49^{+0.17}_{-0.24}$	0.95(149)	–	–
2003-10-07	0148210401	$0.57^{+0.08}_{-0.11}$	$1.37^{+0.20}_{-0.24}$	1.10(150)	–	–
2004-10-06	0164561101	$0.62^{+0.08}_{-0.11}$	$1.40^{+0.13}_{-0.14}$	0.86(263)	$2.12^{+0.26}_{-0.21}$	0.86(69)
2005-03-07	0164561301	$0.70^{+0.07}_{-0.09}$	1.22 ± 0.07	1.08(135)	–	–
2005-10-04	0164561401	$0.65^{+0.04}_{-0.05}$	1.38 ± 0.04	1.15(259)	–	–
2004-09-06	0205350101	$0.66^{+0.05}_{-0.06}$	1.27 ± 0.09	0.99(325)	$2.40^{+0.42}_{-0.31}$	1.03(54)
2006-04-04	0406600301	$0.63^{+0.04}_{-0.05}$	1.23 ± 0.05	1.11(228)	–	–
2006-09-10	0406600401	$0.63^{+0.06}_{-0.07}$	$1.51^{+0.15}_{-0.17}$	1.05(243)	$2.74^{+1.12}_{-0.59}$	0.64(20)
2007-09-26	0502170301	$0.62^{+0.05}_{-0.06}$	$1.59^{+0.18}_{-0.20}$	1.02(211)	$2.20^{+1.15}_{-0.60}$	1.16(8)
2008-04-02	0502170401	$0.60^{+0.05}_{-0.06}$	1.55 ± 0.06	1.16(196)	–	–
2008-09-05	0554600301	$0.54^{+0.04}_{-0.05}$	1.58 ± 0.04	1.19(229)	–	–
2009-03-03	0554600401	$0.53^{+0.05}_{-0.07}$	1.60 ± 0.05	1.04(203)	–	–
2009-09-07	0604090201	$0.52^{+0.04}_{-0.05}$	1.57 ± 0.06	0.91(176)	–	–
2011-03-23	0654230401	$0.52^{+0.04}_{-0.05}$	1.52 ± 0.05	0.92(201)	–	–

Table 4: The spectral results of 1E 1048-5937.

OBS-DATE	OBS-ID	persistent spectrum phabs(BB+BB+PL)				burst spectrum phabs(BB)	
		kT_1(keV)	kT_2(keV)	γ	$red.\chi^2(d.o.f.)$	kT(keV)	$red.\chi^2(d.o.f.)$
2000-12-28	0112780401	0.63 ± 0.05	–	$2.90^{+0.21}_{-0.16}$	1.01(79)	–	–
2003-06-16	0147860101	0.56 ± 0.03	$0.95^{+0.11}_{-0.14}$	$3.58^{+0.34}_{-0.24}$	1.13(225)	$0.62^{+0.12}_{-0.10}$	0.56(19)
2005-06-16	0307410201	0.64 ± 0.02	–	$3.18^{+0.09}_{-0.08}$	0.94(167)	$0.60^{+1.67}_{-0.23}$	0.69(3)
2005-06-28	0307410301	$0.37^{+0.06}_{-0.05}$	$0.72^{+0.05}_{-0.04}$	$6.09^{+2.04}_{-1.40}$	1.22(149)	$0.62^{+0.29}_{-0.18}$	1.56(12)
2007-06-14	0510010601	0.54 ± 0.04	$0.88^{+0.05}_{-0.06}$	$3.43^{+0.39}_{-0.23}$	1.38(250)	$0.60^{+0.06}_{-0.05}$	0.85(44)
2011-08-06	0654870101	$0.43^{+0.05}_{-0.04}$	$0.78^{+0.04}_{-0.03}$	$4.54^{+0.84}_{-0.56}$	1.01(208)	$0.46^{+0.06}_{-0.05}$	0.38(20)

Table 5: The spectral results of SGR 0501+4516.

OBS-DATE	OBS-ID	$N_{\rm H}$	persistent spectrum phabs(BB+PL)			burst spectrum phabs(BB+BB)		
		(10^{22} cm^{-2})	kT (keV)	γ	$red.\chi^2$ ($d.o.f.$)	kT_1 (keV)	kT_2 (keV)	$red.\chi^2$ ($d.o.f.$)
2008-08-29	0552971101	0.84 ± 0.06	0.70 ± 0.01	$2.91^{+0.09}_{-0.10}$	1.14(263)	$0.66^{+0.11}_{-0.10}$	–	0.90(33)
2008-08-31	0552971201	$0.86^{+0.09}_{-0.10}$	0.71 ± 0.02	$2.92^{+0.16}_{-0.17}$	1.12(219)	$0.71^{+0.19}_{-0.15}$	–	1.59(9)
2008-09-02	0552971301	$0.82^{+0.07}_{-0.08}$	0.69 ± 0.01	$2.95^{+0.14}_{-0.14}$	1.18(247)	$0.63^{+0.17}_{-0.13}$	–	0.78(20)
2008-09-30	0552971401	0.84 ± 0.06	0.66 ± 0.01	$3.15^{+0.10}_{-0.11}$	1.05(233)	–	–	–
2008-08-23	0560191501	0.87 ± 0.03	0.70 ± 0.01	2.76 ± 0.05	1.08(249)	0.61 ± 0.03	$2.40^{+0.30}_{-0.23}$	1.13(196)
	0560191501[1][a]	$0.84^{+0.06}_{-0.07}$	0.70 ± 0.02	$2.72^{+0.10}_{-0.11}$	1.03(224)	0.64 ± 0.08	$2.48^{+1.39}_{-0.56}$	1.07(94)
	0560191501[2][a]	0.81 ± 0.07	0.67 ± 0.02	$2.62^{+0.10}_{-0.11}$	1.01(228)	0.66 ± 0.06	$2.79^{+1.04}_{-0.54}$	1.06(118)
	0560191501[3][a]	0.90 ± 0.06	0.71 ± 0.02	$2.83^{+0.09}_{-0.10}$	0.99(225)	$0.49^{+0.07}_{-0.06}$	$1.87^{+0.30}_{-0.21}$	0.94(90)
	0560191501[4][a]	0.94 ± 0.06	0.71 ± 0.02	2.87 ± 0.09	1.22(227)	0.57 ± 0.08	$2.14^{+0.90}_{-0.43}$	1.07(69)
2009-08-30	0604220101	$0.93^{+0.12}_{-0.11}$	0.54 ± 0.02	$4.37^{+0.36}_{-0.30}$	1.19(122)	–	–	–

[a]The same segmentation of observation ID 0560191501 described in Table 2.

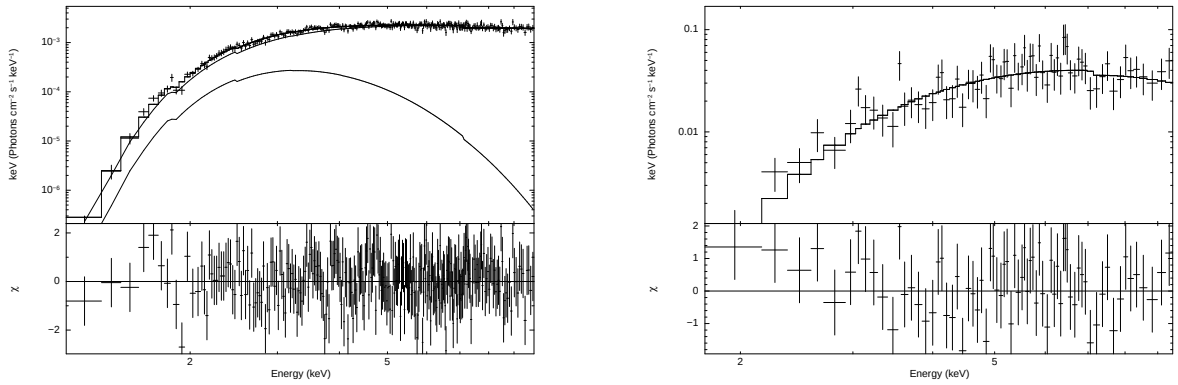

Fig. 1.— The unfolded spectra of persistent emission (left panel) and bursts (right panel) from Obs. ID 0164561101 of SGR 1806-20. We utilized absorbed black body plus power law to fit the persistent emission and a single absorbed black body to fit the bursts.

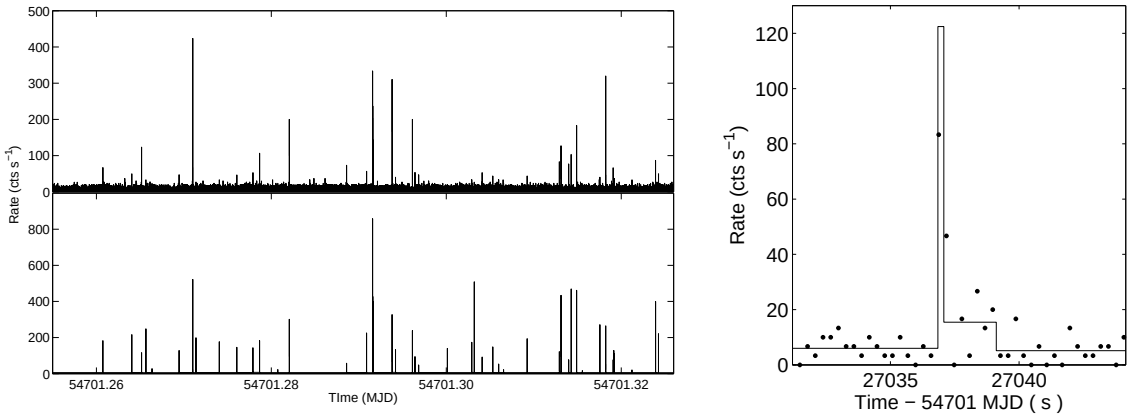

Fig. 2.— The data are from parts of SGR 0501+4516's first observation (Obs. ID 0560191501). Left panel: the photon count rates with 0.3 s bin (top) and the short burst results (bottom) of Bayesian blocks algorithm. The duration is about 6000 s. Right panel: one detected short burst in 10 s observation. The dots are the 0.3 s bin data, while the solid line is the result of Bayesian block algorithm.

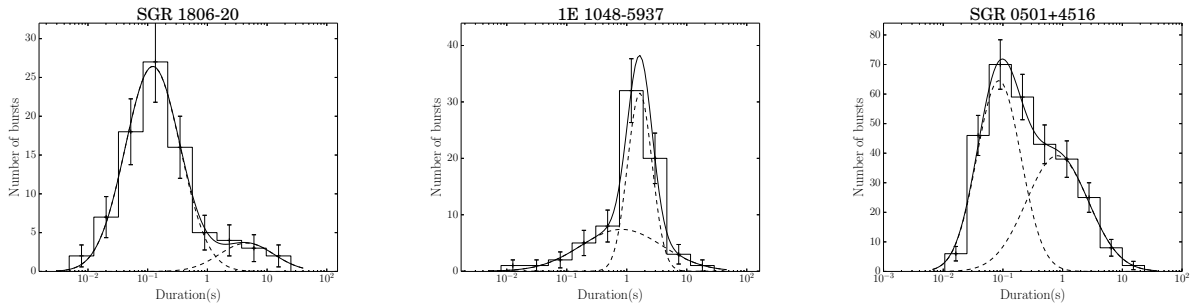

Fig. 3.— The duration distributions for SGR 1806-20, 1E 1048-5937 and SGR 0501+4516 from left to right, respectively. The solid lines are the best fit of the histogram with a sum of two lognormal functions, while the dashed lines are the two components respectively.

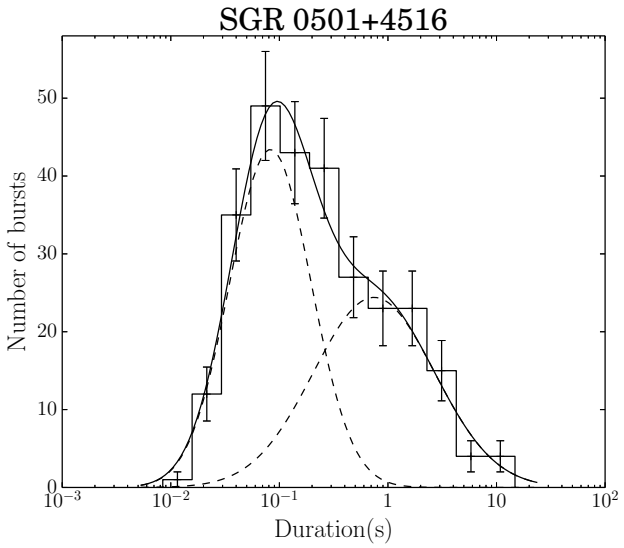

Fig. 4.— This figure shows the duration distribution of the first observation from SGR 0501+4516 to make a comparison with the results from Lin et al. (2013). The solid line represents the best fit by two lognormal functions, while the dashed lines represent the two components respectively.

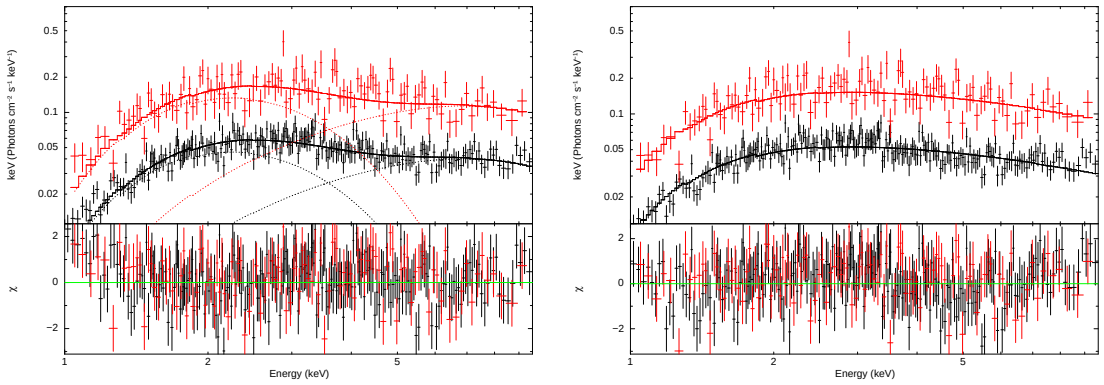

Fig. 5.— The spectra of shorter time scale bursts (< 0.2 s) with high normalization and longer time scale bursts (≥ 0.2 s) with low normalization for SGR 0501+4516, respectively. Both of them can be well fitted by two black body components (left), or by OTTB (right).

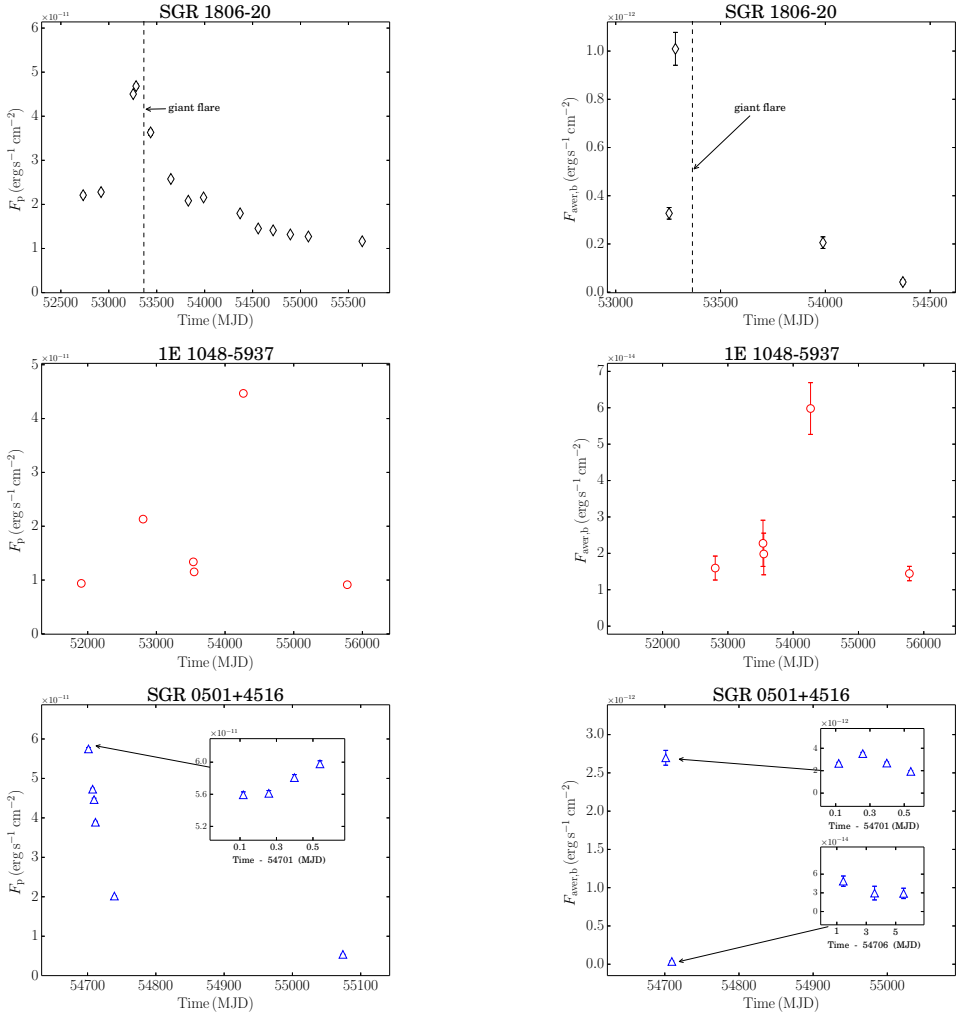

Fig. 6.— The left panels display the persistent flux evolution. The black diamonds, the red circles, the blue triangles represent the persistent flux of SGR 1806-20, 1E 1048-5937 and SGR 0501+4516, respectively (same as Fig. 7). The right panels show the average burst flux, only for those observations have more than 50 burst photons, with the same symbols as left panels. Particularly for the SGR 0501+4516, some points are too near to be distinguished, so we calculated the mean value of them and showed the variations in the inside panels.

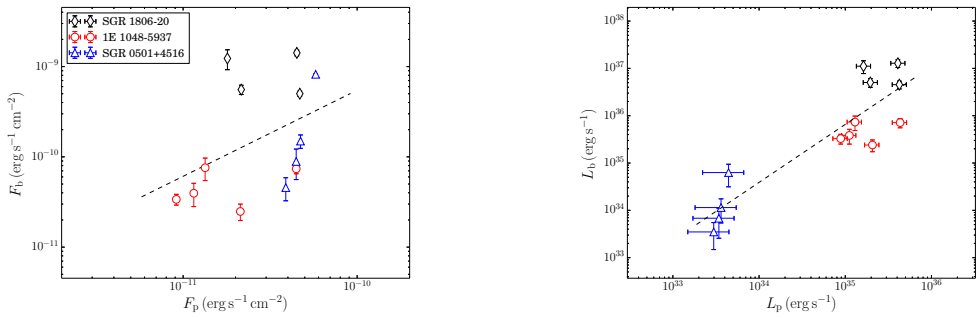

Fig. 7.— The black diamond, the red circle and the blue triangle represent SGR 1806-20, 1E 1048-5937 and SGR 0501+4516 respectively. The dashed lines are the fitted power laws described in Section 4.3.

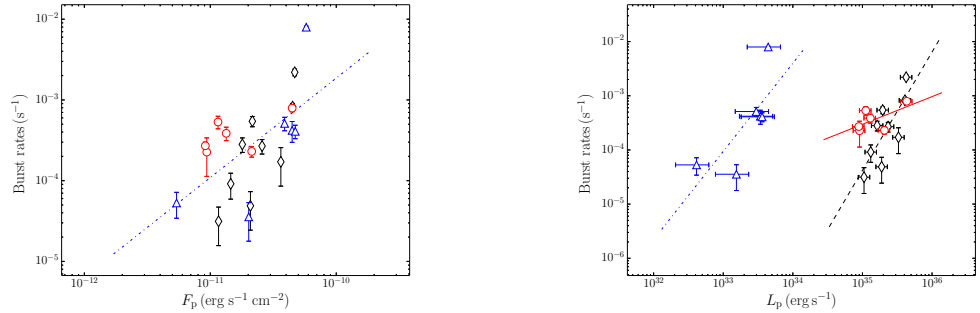

Fig. 8.— Left panel, the relationship between the burst rate and the persistent luminosity. Right panel, three power laws are fitted for SGR 1806-20, 1E 1048-5937 and SGR 0501+4516, shown as dashed line, solid line and dot-dashed line, respectively.

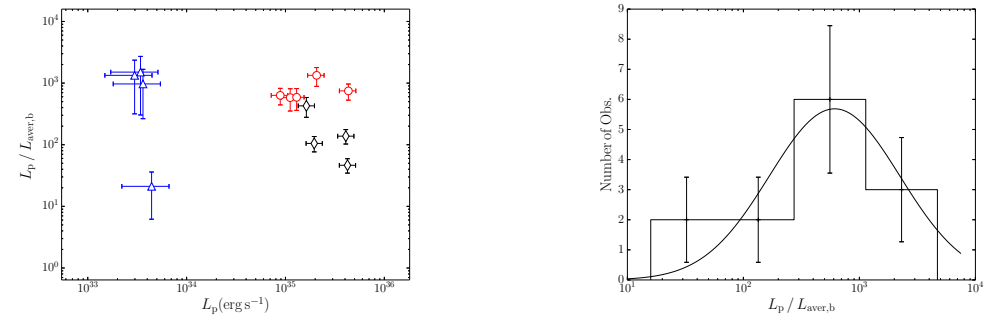

Fig. 9.— In the left panel, the symbols are the same as Fig. 7. It shows the correlation between the ratio (L_p/L_b) and the persistent luminosity. The right panel shows the distribution of the ratio of 13 observations from all three sources. The solid line shows the best fit result with lognormal function.